Improving Accuracy of Wall-Normal Derivatives for Anisotropic Adaptive Simplex-Element Grids

Matthew D. O'Connell*, Jeffery A. White†, Michael A. Park‡, Kyle B. Thompson§
NASA Langley Research Center, Hampton VA 23681
and
Hiroaki Nishikawa¶
National Institute of Aerospace, Hampton, VA 23666, USA

In this paper, we explore methods for computing wall-normal derivatives used for calculating wall skin friction and heat transfer over a solid wall in unstructured simplex-element (triangular/tetrahedral) grids generated by anisotropic grid adaptation. Simplex-element grids are considered as suitable for automatic grid generation and adaptation, but present a challenge to accurately predict wall-normal derivatives. For example, wall-normal derivatives computed by a simple finite-difference approximation, as typically done in practical fluid-dynamics simulation codes, are often contaminated with numerical noise. Because of nonuniform cell heights that are typically produced by adaptive meshing, velocity profiles are sampled at irregular distances away from the surface so that even if a profile were constant across the entire surface, oscillations in the skin frictions would be observed. To address this issue, we propose a new method based on a common step-length for the finite-difference approximation, which is expected to smooth the wall-normal derivative distribution over a boundary. Also, we consider using least-squares gradients to compute the wall-normal derivatives and discuss their possible improvements. Numerical results show that the improved methods greatly reduce the noise in the wall-normal derivatives for irregular simplex-element grids.

1. Introduction

Towards fully automated computational fluid dynamics (CFD) simulations, there is an increasing interest in developing robust and accurate discretizations and solvers for unstructured simplex-element grids with anisotropic grid adaptation [1–6]. While fully-automated CFD simulations have recently been successfully demonstrated for practical three-dimensional problems [2, 7], improvements are still desired in the discretization method, especially in terms of accuracy. For example, computations of derivatives such as the viscous/heat fluxes and the vorticity are known to suffer from numerical noise on highly irregular and skewed simplex-element grids [8]. Impact of numerical noise may be reduced in integrated quantities (e.g., drag coefficient), but when accuracy is required for a pointwise quantity, e.g., heating rate at a stagnation point, numerical noise can be a serious problem, causing a large error and a great degree of uncertainty in the prediction. A reliable automated CFD simulation tool must be able to accurately predict pointwise derivatives, on irregular anisotropic simplex-element grids, especially at wall boundaries.

There have been efforts to improve derivative accuracy on unstructured grids: directly solving for gradients as part of the solution process [8, 9], improved least-squares methods [10–12], and implicit gradient methods [13,14]. All these methods are promising for improving derivative accuracy, but they are not specifically designed to accurately estimate derivatives at a boundary, and thus, further improvements may be

*Research Scientist, (matthew.d.oconnell@nasa.gov) Computational AeroSciences, AIAA Member.
†Senior Research Scientist, (jeffery.a.white@nasa.gov) Computational AeroSciences, Associate Fellow AIAA
‡Research Scientist, (mike.park@nasa.gov), Computational AeroSciences, Associate Fellow AIAA
§Research Scientist, (kyle.b.thompson@nasa.gov), Computational Aerothermodynamics, Associate Fellow AIAA
¶Associate Research Fellow (hiro@nianet.org), 100 Exploration Way, Hampton, VA 23666 USA, Associate Fellow AIAA

achieved by developing a more specific technique. In this work, we focus on wall-normal derivatives and explore various methods for accurately estimating the wall-normal derivatives relevant to the viscous stresses and heat fluxes at a wall, as a post-processing step for a given numerical solution on adaptive simplex-element grids. A popular technique used in practical CFD codes for computing the wall-normal derivatives is a one-sided finite-difference formula applied in the wall-normal direction with the numerical solution in a nearby node/cell and a boundary condition value. For example, it provides an approximation to $\partial u/\partial n$ that dominates the viscous stress at a wall, where u is a wall-parallel velocity component and n is the coordinate normal to the wall. It can provide an accurate approximation on structured grids, but will introduce numerical noise on irregular simplex-element grids [1]. We conjecture that the numerical noise in the derivative is due to the irregularity of the spacing used in the finite-difference form. That is, the distance between the center of a cell adjacent to a boundary and a wall-boundary face centroid varies along a boundary in adaptive simplex-element grids. Thus, we propose to keep the same distance for the finite-difference formula applied at all wall-boundary faces. Numerical experiments show that the modified finite-difference method greatly improves the skin friction distribution over a flat plate in a laminar flow, where the distance is determined as $\eta = 0.5$ at all boundary faces, where η is a normalized coordinate in the Blasius boundary-layer solution. To extend this technique to more general flows over complex geometries, it is necessary to develop a method for estimating a universal distance for the finite-difference formula. We plan to explore various methods, and present results in the final paper.

Another post-processing technique can be devised based on gradients computed by a least-squares method at nodes or cells. Following a recent study [1], where heating rate prediction over a flat plate in a hypersonic turbulent flow has been shown to be greatly improved by the face-averaged nodal-gradient (F-ANG) approach applied to the finite-volume discretization [1, 15], we employ the F-ANG approach in this study, but only consider it as a post-processing technique for estimating the wall-normal derivatives for a given numerical solution. Discussions on the impact of the gradient approach (used in the discretization) on wall heating prediciton are given in a companion paper [16]. In the F-ANG method, gradients are computed and stored at nodes while numerical solutions are stored at cells. Therefore, the wall-normal derivatives are already available at wall nodes. However, these derivatives can be noisy for irregular anisotropic simplex-element grids. A simple method for reducing the noise would be to average the nodal gradients, and there are two possible techniques: face and cell averages. We compare these averaged gradients for estimating the wall-normal derivatives. Numerical results indicate that the cell-averaged nodal-gradients can greatly reduce the noise in the wall-normal derivatives, but not as much as the improved finite-difference formula presented here.

2. Finite-Volume Discretization

In Figure 1 consider a cell-centered finite-volume discretization for the Navier-Stokes equations integrated over a computational cell j with the midpoint rule:

$$\mathbf{Res}_j = \sum_{k \in \{k_j\}} \mathbf{\Phi}_{jk} A_{jk}, \tag{2.1}$$

where $\{k_j\}$ is a set of neighbors of the cell j, A_{jk} is the length of the face across j and k, and $\mathbf{\Phi}_{jk}$ is a numerical flux. In this work, the Roe flux [17] is used for the inviscid terms, and the alpha-damping flux [18] for the viscous terms. The solution values are stored in the primitive variables $\mathbf{w} = (\rho, \mathbf{v}, T)$, at cells as point values at the centroid [4], where ρ is the density, $\mathbf{v}$ is the velocity vector, and T is the temperature. Second-order accuracy is achieved by the linearly-exact flux quadrature (i.e., the midpoint rule) and the numerical flux evaluated with linearly reconstructed solutions. In this work, we focus on the F-ANG approach [1, 15], which has been shown to yield significantly more accurate wall-derivatives than a conventional finite-volume scheme, but still involves mild oscillations in the derivatives on irregular simplex-element grids. In the F-ANG approach, we compute the solution gradients at nodes by using solution values stored at cells by a linear least-squares method. Then, the nodal gradients are used in the linear reconstruction, averaged over the nodes of a face:

$$\mathbf{w}_L = \mathbf{w}_j + \nabla \mathbf{w}_f \cdot \Delta \mathbf{x}_{jm}, \quad \mathbf{w}_R = \mathbf{w}_k + \nabla \mathbf{w}_f \cdot \Delta \mathbf{x}_{km}, \tag{2.2}$$

where $\nabla \mathbf{w}_f$ denotes the face-averaged gradient:

$$\nabla \mathbf{w}_f = \frac{1}{2}\left(\nabla \mathbf{w}_{jk}^{\ell} + \nabla \mathbf{w}_{jk}^{r}\right), \tag{2.3}$$

where the superscripts ℓ and r denote the left and right nodes of the face $[j,k]$ (see Figure 1). This approach has various advantages especially for simplex-element grids, e.g., no interpartition data are required for gradients, and the residual stencil is greatly reduced. For further details see Refs. [1, 15].

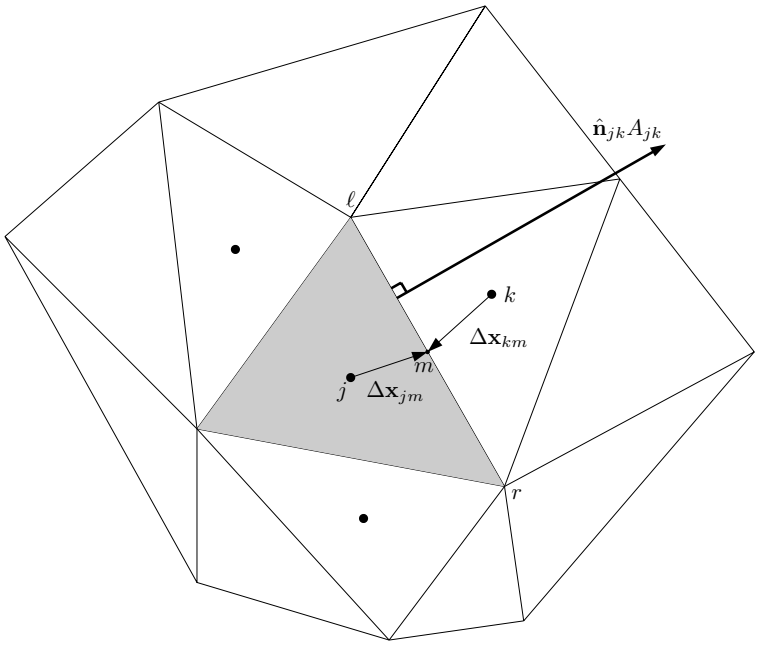


Figure 1: Stencil for cell-centered finite-volume discretization.

3. Methods for Computing Wall-Normal Derivatives

In this section, we describe methods for computing a wall-normal derivative, taking the velocity derivative $\partial u/\partial n$ as an example, where u is the wall-parallel component of the velocity and n denotes the coordinate normal to the wall. We assume that the value at a wall u_b is known, e.g., $u_b = 0$ for a no-slip condition. The wall-normal derivative will be computed at a boundary node or at a boundary face, depending on the method.

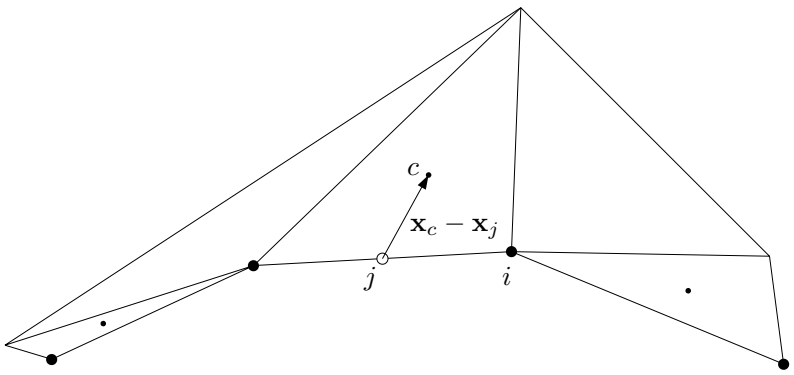


Figure 2: Geometry of an irregular triangular grid over a boundary. Large black filled circles are boundary nodes; smaller circles are the centroids of triangles adjacent to the boundary.

3.1. Nodal Gradients

The wall-normal derivative is computed at a boundary node i by projecting the nodal gradient ∇u_i in the direction of wall normal as depicted in Figure 2:

$$\left.\frac{\partial u}{\partial n}\right|_i = \nabla u_i \cdot \hat{\mathbf{n}}_i, \tag{3.1}$$

where $\hat{\mathbf{n}}_i$ denotes a unit vector at the node i normal to the wall pointing towards the interior domain. The normal at the node is computed by averaging the normal vectors of faces adjacent to the node that have a wall boundary condition. This is perhaps the simplest method since the nodal gradients are already available from the F-ANG method used in the underlying discretization.

3.2. Face-Averaged Nodal Gradients

The wall-normal derivative is computed at a face j with a face-averaged gradient:

$$\left.\frac{\partial u}{\partial n}\right|_j = \overline{\nabla} u_j^{face} \cdot \hat{\mathbf{n}}_j, \tag{3.2}$$

where $\overline{\nabla} u_j^{face}$ is the average of the nodal gradients over the boundary face j. In Figure 2, $\overline{\nabla} u_j^{face}$ is obtained by averaging the nodal gradients at the left and right nodes of the boundary face j.

3.3. Cell-Averaged Nodal Gradients

The wall-normal derivative is computed at a face j with a cell-averaged gradient:

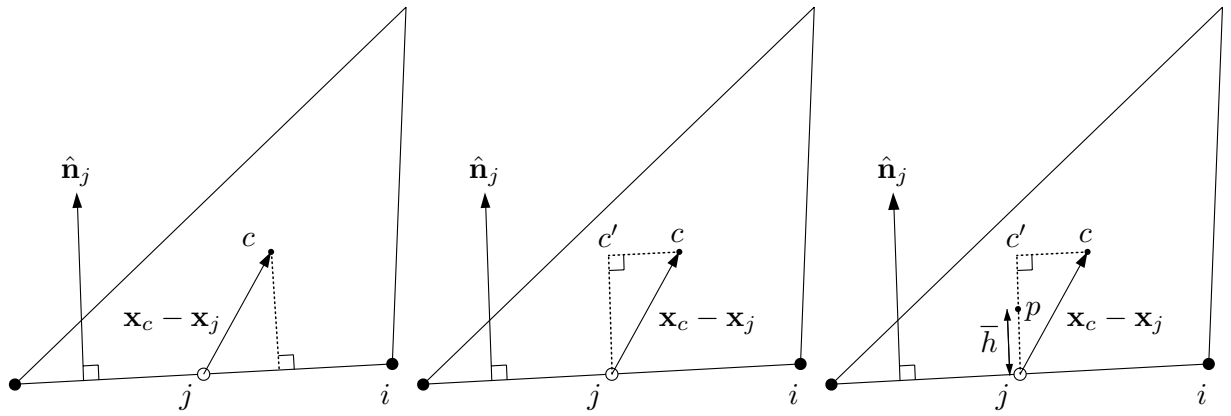
$$\left.\frac{\partial u}{\partial n}\right|_j = \overline{\nabla} u_j^{cell} \cdot \hat{\mathbf{n}}_j, \tag{3.3}$$

where $\overline{\nabla} u_j^{cell}$ is the average of the nodal gradients over a cell adjacent to the face j. In Figure 2, $\overline{\nabla} u_j^{cell}$ is obtained by averaging the nodal gradients at the three nodes of the triangular cell c.

3.4. Finite-difference I

The wall-normal derivative can be computed at a face j by the following finite-difference formula:

$$\left.\frac{\partial u}{\partial n}\right|_j = \frac{u_c - u_b}{(\mathbf{x}_c - \mathbf{x}_j) \cdot \hat{\mathbf{n}}_j}, \tag{3.4}$$



(a) Finite-difference I. (b) Finite-difference II. (c) Finite-difference III.

Figure 3: Geometries for the finite-difference wall-normal derivative formulas.

where u_c is a solution value stored at the cell c adjacent to the boundary face j, u_b is a known boundary value (e.g., from a boundary condition), $\mathbf{x}_c$ is the centroid position of the cell c, $\mathbf{x}_j$ is the centroid of the boundary face j. See Figure 3(a). This formula estimates the derivative at a point where the cell-center $\mathbf{x}_c$ is projected on the boundary, not at $\mathbf{x}_j$.

3.5. Finite-difference II

The wall-normal derivative can be estimated at the face centroid by

$$\left.\frac{\partial u}{\partial n}\right|_j = \frac{u_{c'} - u_b}{(\mathbf{x}_c - \mathbf{x}_j) \cdot \hat{\mathbf{n}}_j}, \tag{3.5}$$

where $u_{c'}$ is a solution extrapolated from the cell center $\mathbf{x}_c$ to the point right above the face centroid (see Figure 3(b)):

$$u_{c'} = u_c + \nabla u_c \cdot (\mathbf{x}_{c'} - \mathbf{x}_c), \quad \mathbf{x}_{c'} = \mathbf{x}_j + [(\mathbf{x}_c - \mathbf{x}_j) \cdot \hat{\mathbf{n}}_j]\hat{\mathbf{n}}_j. \tag{3.6}$$

This approximation is exact for linear functions at the face centroid.

3.6. Finite-difference III

In the previous methods, the finite-difference formula is applied with varying step-length as the distance between the cell center and the face center in the normal direction changes randomly on irregular simplex-element grids. Hence, the methods are strongly dependent on the grid geometry, which is not suitable for adaptive simplex-element grids. To minimize the dependence on the grid geometry, we generalize the previous formula as

$$\left.\frac{\partial u}{\partial n}\right|_j = \frac{u_p - u_b}{\overline{h}}, \tag{3.7}$$

where u_p is a solution extrapolated from the cell center $\mathbf{x}_c$ to the point at a certain distance $\overline{h}$ from the face center in the wall normal direction (Figure 3(c)):

$$u_p = u_c + \nabla u_c \cdot (\mathbf{x}_p - \mathbf{x}_c), \quad \mathbf{x}_p = \mathbf{x}_j + \overline{h}\,\hat{\mathbf{n}}_j, \tag{3.8}$$

where $\overline{h}$ is a global constant or varies along a wall but constant in a transformed normal coordinate. This approximation is also exact for linear functions at the face centroid.

This formula does not depend strongly on the cell centroids of the adjacent cells. Whether in the physical or transformed coordinate, the above formula keeps the same step-length of the finite-difference formula over a wall and thus is expected to produce a smoother derivative, and a smoother error distribution.

In this work, we investigate the effects of a common step-length $\overline{h}$ and explore estimation techniques of $\overline{h}$ for various viscous-flow problems on adaptive grids. In this abstract, we provide preliminary results for a laminar flat-plate computation with the height $\overline{h}$ determined as described below.

4. Numerical Results

4.1. Two-Dimensional Laminar Flat Plate at $M_\infty = 0.15$, $Re_\infty = 10^6$

For a laminar flat plate, we consider the normalized wall-normal coordinate η:

$$\eta = \frac{y}{x}\sqrt{Re_x}, \quad Re_x = \frac{\rho_\infty U_\infty x}{\mu_\infty}, \tag{4.1}$$

where x is the distance from the leading edge, ρ_∞, U_∞, μ_∞ are freestream density, flow speed, and viscosity. For the finite-difference III, we fix the height to be $\eta = 0.5$, which is translated into the y-coordinate as

$$\overline{h} = \eta \frac{x_j}{\sqrt{Re_\infty}}, \tag{4.2}$$

where $\eta = 0.5$, x_j is the x-coordinate of the face centroid, and Re_∞ is the freestream Reynolds number per unit length. Note that in finite-difference III we only compute the wall-normal velocity derivative at boundary face centroids. The test grid used has a node at the $x = 0.0$ location; and thus, x_j will not be zero on any face centroid. As can be seen from the formula, the height $\overline{h}$ changes in the physical coordinate parabolically but remains constant in the normalized wall-normal coordinate η. In the results, this method is denoted by FD-III($\eta = 0.5$). For a more general flow problem, this approach may not be suitable. Therefore, we also consider using a fixed length over the wall in the physical space:

$$\overline{h} = \eta\sqrt{Re_\infty}, \tag{4.3}$$

which corresponds to using the estimated distance with $\eta = 0.5$ at $x_j = 1.0$ everywhere. In this case, $\overline{h}$ is a global constant.

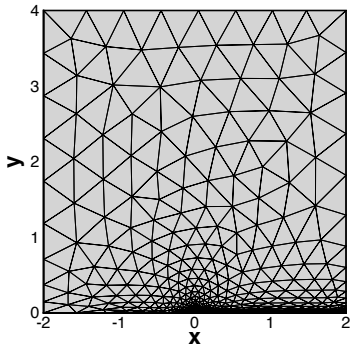
An adaptive grid was generated by the open-source tool *refine* [19]. The Navier-Stokes equations were solved using a F-ANG based finite-volume solver. A least-squares method was used from the cell-based solution to compute a Mach Hessian at the nodes. Adaptation was then performed with the multiscale metric technique ([20]) to control interpolation error in the L2-norm in the Mach field. The resulting adaptive grid is shown in Figures 4(a) and 4(b). As can be seen, it is a fully irregular grid towards the flat plate located at the bottom in $x \in [0, 2]$. Note that we already have a numerical solution on this grid as shown by Mach contours in Figure 4(b). Then, the skin friction is computed at the flat plate as

$$C_{fx} = (\tau_{xx}, \tau_{xy}) \cdot \hat{\mathbf{n}} \frac{2}{M_\infty^2} = \mu \left(\frac{2}{3}\frac{\partial u}{\partial x} - \frac{1}{3}\frac{\partial v}{\partial y}, \frac{\partial u}{\partial y} + \frac{\partial v}{\partial x} \right) \cdot \hat{\mathbf{n}} \frac{2}{M_\infty^2} = \mu \left(\frac{\partial u}{\partial y} + \frac{\partial v}{\partial x} \right) \frac{2}{M_\infty^2}, \tag{4.4}$$

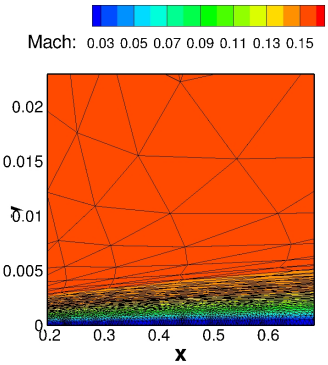
where u and v are the x- and y-components of the velocity, the factor $1/M_\infty^2$ comes from the nondimensionalization (i.e., the velocity is nondimensionalized by the freestream speed of sound), and $\hat{\mathbf{n}}$ is either $\hat{\mathbf{n}}_i$ or $\hat{\mathbf{n}}_j$, depending on where the gradients are computed. The term $\partial v/\partial x$ is ignored in the finite-difference methods, but retained in the LSQ gradient methods.

Results are shown in Figures 4(c)–4(i), where numerical skin-friction distributions are compared with that of the Blasius solution. All numerical skin-friction distributions are close to the theoretical distribution on average, but significant differences are observed in the noise level. First, the FD-I and FD-II methods produce noisy skin-friction distributions as shown in Figures 4(c) and 4(d). On the other hand, the proposed methods produce much smoother distributions as shown in Figures 4(e) and 4(f). Note that the choice of $\overline{h}$ has no major impact on the skin-friction distribution: Figure 4(e) for $\eta = 0.5$, and Figure 4(f) for a global constant corresponding to $\eta = 0.5$ and $x = 1$. These results indicate that it is the uniformity of the step-length, whether in η or y, that affects the smoothness of the skin friction distribution. This is encouraging since the method can be extended to more general problems by developing a method for estimating a single value of the step-length $\overline{h}$ in a given physical problem.

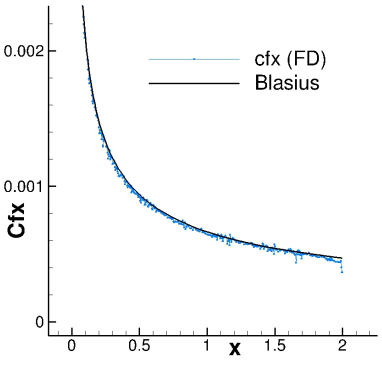
For the LSQ gradient methods, the direct use of the nodal gradients leads to a noisy skin-friction distribution as shown in Figure 4(g). A slightly smoother distribution is obtained with the face-averaged nodal gradients as shown in Figure 4(h). The smoothest distribution is obtained with the cell-averaged nodal gradients as shown in Figure 4(i). The results indicate that averaging with more nodal gradients leads to a smoother distribution, but not as smooth as those obtained with the finite-difference III. Note that the gradients are linearly exact no matter how they are averaged, and the averaging operator acts as a kind of filtering to remove high-frequency contents from the underlying gradient approximation.



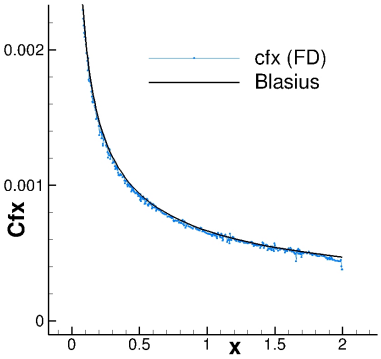
(a) Adaptive grid (3457 nodes).



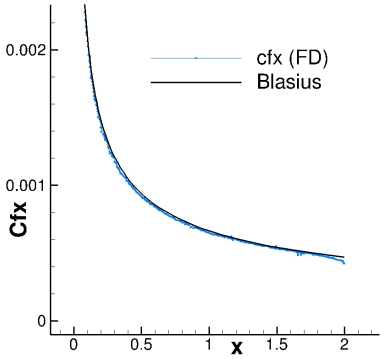
(b) Zoomed-in view of the grid (with a scaled y-coordinate) and Mach contours.



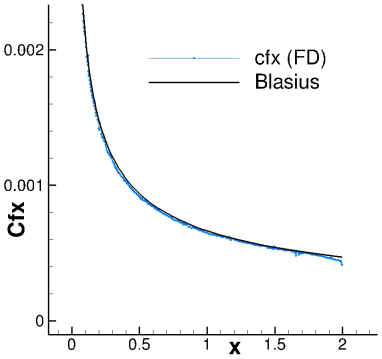
(c) FD-I.



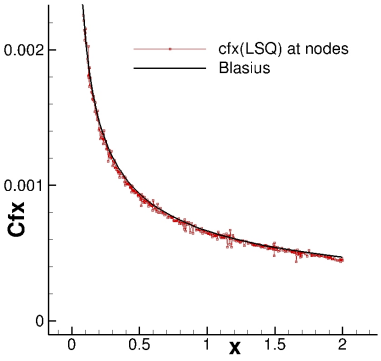
(d) FD-II.



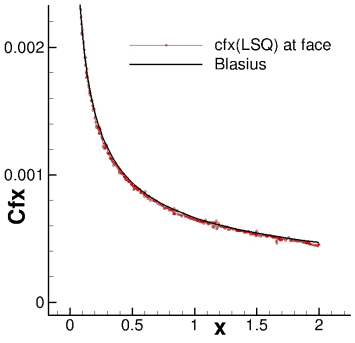
(e) FD-III ($\eta = 0.5$).



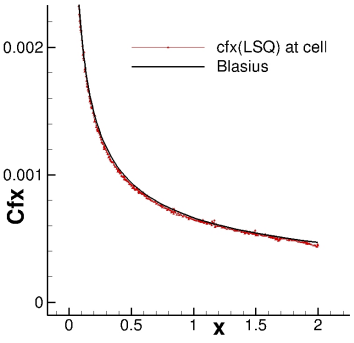
(f) FD-III ($\eta = 0.5$, $x = 1$).



(g) Nodal gradients.



(h) Face-averaged gradients.



(i) Cell-averaged gradients.

Figure 4: Results for a laminar flow over a flat plate at $M_\infty = 0.15$ and $Re_\infty = 10^6$ on an adaptive triangular grid. The flat plate is located at $y = 0$ in $x \in [0, 2]$. The skin friction coefficient C_{fx} is plotted at wall face centers, except for the figure (g).

5. Final Paper

In the final paper, we plan to add a discussion on the estimation of $\overline{h}$ for three-dimensional turbulent flows, and numerical results for comparing various wall-normal-derivative methods in the prediction of skin friction and heating rate in a three-dimensional hypersonic turbulent flow.

Acknowledgments

This work was supported by the Hypersonic Technology Project, through the Hypersonic Airbreathing Propulsion Branch of the NASA Langley Research Center, under Contract No. 80LARC17C0004.

References

[1]White, J., Nishikawa, H., and Baurle, R., "A 3-D Nodal-Averaged Gradient Approach for Unstructured-Grid Cell-Centered Finite-Volume Methods for Application to Turbulent Hypersonic Flow," *SciTech 2020 Forum*, AIAA Paper 2020-0652, Orlando, FL, 2020.

[2]Kleb, W. L., Park, M. A., Wood, W. A., Bibb, K. L., Thompson, K. B., and Gomez, R. J., "Sketch-to-Solution: An Exploration of Viscous CFD with Automatic Grids," *24th AIAA Computational Fluid Dynamics Conference*, AIAA Paper 2019-2948, Dallas, TX, 2019.

[3]Nishikawa, H., "A Face-Area-Weighted Centroid Formula for Reducing Grid Skewness and Improving Convergence of Edge-Based Solver on Highly-Skewed Simplex Grids," *SciTech 2020 Forum*, AIAA Paper 2020-1786, Orlando, FL, 2020.

[4]Nishikawa, H., "A Face-Area-Weighted Centroid Formula for Finite-Volume Method That Improves Skewness and Convergence on Triangular Grids," *J. Comput. Phys.*, Vol. 401, 2020, pp. 109001.

[5]Park, M. A., Barral, N., Ibanez, D., Kamenetskiy, D. S., Krakos, J. A., Michal, T. R., and Loseille, A., "Unstructured Grid Adaptation and Solver Technology for Turbulent Flows," *56th AIAA Aerospace Sciences Meeting*, AIAA Paper 2018-1103, Kissimmee, Florida, 2018.

[6]Alauzet, F. and Loseille, A., "A Decade of Progress on Anisotropic Mesh Adaptation for Computational Fluid Dynamics," *Computer-Aided Design*, March 2015, pp. 13–39.

[7]Kleb, W. L., Schoenenberger, M., Korzun, A. M., and Park, M. A., "Sketch-to-Solution: A Case Study in RCS Aerodynamic Interaction," *25th AIAA Computational Fluid Dynamics Conference*, AIAA Paper 2020-0673, Orlando, FL, 2020.

[8]Liu, Y. and Nishikawa, H., "Third-Order Inviscid and Second-Order Hyperbolic Navier-Stokes Solvers for Three-Dimensional Inviscid and Viscous Flows," *46th AIAA Fluid Dynamics Conference*, AIAA Paper 2016-3969, Washington, D.C., 2016.

[9]Nishikawa, H., "A Hyperbolic Poisson Solver for Tetrahedral Grids," *J. Comput. Phys.*, Vol. 409, May 2020, pp. 109358.

[10]Xiong, M., Deng, X., Gao, X., Dong, Y., Xu, C., and Wang, Z., "A Novel Stencil Selection Method for the Gradient Reconstruction on Unstructured Grid Based on OpenFOAM," *Comput. Fluids*, Vol. 172, 2018, pp. 426–442.

[11]Sozer, E., Brehm, C., and Kiris, C. C., "Gradient Calculation Methods on Arbitrary Polyhedral Unstructured Meshes for Cell-Centered CFD Solvers," *Proc. of 52nd AIAA Aerospace Sciences Meeting*, AIAA Paper 2014-1440, National Harbor, Maryland, 2014.

[12]Shima, E., Kitamura, K., and Haga, T., "Green-Gauss/Weighted-Least-Squares Hybrid Gradient Reconstruction for Arbitrary Polyhedra Unstructured Grids," *AIAA J.*, Vol. 51, No. 11, 2013, pp. 2740–2747.

[13]Wang, Q., Ren, Y.-X., Pan, J., and Li, W., "Compact High Order Finite Volume Method on Unstructured Grids III: Variational Reconstruction," *J. Comput. Phys.*, Vol. 337, 2017, pp. 1–26.

[14]Nishikawa, H., "From Hyperbolic Diffusion Scheme to Gradient Method: Implicit Green-Gauss Gradients for Unstructured Grids," *J. Comput. Phys.*, Vol. 372, 2018, pp. 126–160.

[15]Nishikawan, H. and White, J. A., "An Efficient Cell-Centered Finite-Volume Method with Face-Averaged Nodal-Gradients for Triangular Grids," *J. Comput. Phys.*, Vol. 411, 2020, pp. 109423.

[16]White, J. A. and Nishikawa, H., "Computation of the Wall Heat Flux for a Hypersonic Flow Using Tetrahedral Grids," *AIAA SciTech*, 2021, to be published as AIAA paper.

[17]Roe, P. L., "Approximate Riemann Solvers, Parameter Vectors, and Difference Schemes," *J. Comput. Phys.*, Vol. 43, 1981, pp. 357–372.

[18]Nishikawa, H., "Beyond Interface Gradient: A General Principle for Constructing Diffusion Schemes," *Proc. of 40th AIAA Fluid Dynamics Conference and Exhibit*, AIAA Paper 2010-5093, Chicago, 2010.

[19]Park, M. A. and Darmofal, D. L., "Parallel Anisotropic Tetrahedral Adaptation," *Proc. of 46th AIAA Aerospace Sciences Meeting and Exhibit*, AIAA Paper 2008-917, Reno, Nevada, 2008.

[20]Park, M. A., Balan, A., Anderson, W. K., Galbraith, M. C., Caplan, P. C., Carson, H. A., Michal, T., Krakos, J. A., Kamenetskiy, D. S., Loseille, A., Alauzet, F., Frazza, L., and Barral, N., "Verification of Unstructured Grid Adaptation Components," AIAA Paper 2019–1723, 2019.